Tripeptide-assisted gold nanocluster formation for sensing Fe^{3+} and Cu^{2+}

Jonghae Youn[2,3], Peiyuan Kang[3], Justin Crowe[1], Caleb Thornsbury[1], Peter Kim[2], Zhenpeng Qin[3,4,5,6], Jiyong Lee*[1]

1. Department of Chemistry and Biochemistry, The University of Texas at Tyler, Tyler, TX, United States.
2. Department of Chemistry and Biochemistry, The University of Texas at Dallas, Richardson, TX, United States.
3. Department of Mechanical Engineering, The University of Texas at Dallas, Richardson, TX, United States.
4. Department of Bioengineering, The University of Texas at Dallas, Richardson, TX, United States.
5. Department of Surgery, The University of Texas at Southwestern Medical Center, Dallas, TX, United States.
6. Center for Advanced Pain Studies, The University of Texas at Dallas, Richardson, TX, United States.
*Correspondence: jiyonglee@uttyler.edu

Abstract

Over the past decade, various fluorescent gold nanoclusters (AuNCs) have been studied for their potential as metal ion sensors. Due to the importance of the surface ligand in stabilizing nanocluster and sensing target metal ions, there is a great need of further investigations into possible surface ligands to develop selective and sensitive sensors. In this study, we designed very simple tripeptides to form fluorescent AuNCs by taking advantage of the reduction capability of tyrosine under alkaline conditions. In addition to studying the role of tyrosine in forming AuNC, we also investigated the role of tyrosine in sensing metal ions. Two tripeptides, tyrosine-cysteine-tyrosine (YCY) and serine-cysteine-tyrosine (SCY), were prepared and used for the formation of AuNCs. We obtained AuNCs with blue and red fluorescence from YCY peptides and AuNCs with blue fluorescence from SCY peptides. We

found that the fluorescence of blue fluorescence-emitting YCY- and SCY-AuNCs is selectively quenched with Fe^{3+} and Cu^{2+}, while the fluorescence of the red fluorescence-emitting YCY-AuNC is stable with 13 different metal ions. We have observed that the number of tyrosine residues affects the response of sensors. In the presence of different metal ions, different aggregation propensities were observed from DLS measurement. These results suggest the chelation between the peptide on the AuNC surface and the target ions results in aggregation and causes fluorescence quenching. Our study has shown that very simple and short peptides can be designed rationally for the formation of fluorescent AuNCs and utilized as the surface ligand for the metal ion sensing.

Introduction

Ultrasmall gold nanoclusters (AuNCs) comprising several gold atoms have gained great interest in the field of catalysis, bioimaging, optical sensing, and biomedicine due to their unique physical and optoelectronic properties, such as ultrasmall sizes, large Stokes shift, longer fluorescence lifetimes, photostability, biocompatibility, and feasibility of surface functionalization.[1-7] When the size of AuNC approaches the Fermi wavelength (~ 1 nm) of the electrons, the continuous band of energy breaks into discrete electron transition energy levels, exhibiting the single molecule-like fluorescence.[8-11] The electrons filled in $5d^{10}$ of the valence band are excited to $6sp^1$ of the conduction band, thereby display a strong fluorescence emission from the visible to the near-infrared region.[10]

There are two common strategies, bottom-up and top-down, for the preparation of fluorescent AuNCs. The bottom-up approach is to reduce the Au ions to the Au atoms through chemical, biological, optical, and electrochemical reduction of the Au ions. However, due to the aggregation propensity of AuNCs, suitable surface ligands acting as stabilizers, such as small thiol molecules, polymers, peptides, and proteins are essential for the preparation of stable AuNCs.[12-15] In the top-down approach, on the other hand, larger gold nanoparticles (~ 100 nm) are etched by adding excess amount of etching agents, such as polyethylenimine (PEI), dihydrolipoic acid (DHLA), or glutathione (GSH) to generate AuNCs.[16-18]

Several synthetic methods for generating fluorescent AuNCs have been developed using ligands acting as both reducing agent and stabilizer. Such ligands include proteins, peptides, polymers, and DNA.[19-23] Proteins are preferred surface ligands due to the roles that several amino acids play in AuNC formation. Thiol group in cysteine residue binds to Au precursor (Au^{3+}) *via* strong Au-S bonds. The phenol group of tyrosine can reduce the Au^{3+} into Au^{0} especially under alkaline condition. By electron transfer, the phenol group of tyrosine becomes a semi-quinone.[24-27] Based on these previous observations, we have hypothesized a very short peptide such as tripeptide with a cystine and tyrosine in the sequence would be enough for efficient fluorescent AuNC formation.

AuNCs have become promising tools for the development of chemical sensors. The straightforward detection, high responsiveness, minimum sample requirement, and real time monitoring capability with fast response time make them excellent sensing systems for detecting highly mutagenic metal ions such as Hg^{2+}, Fe^{3+}, Cu^{2+}, Pb^{2+}, and Cr^{3+}.[28-33] Most of the detections were based on the fluorescence quenching of AuNCs in the presence of target metal ions.[28, 34, 35] In sensing mechanisms known to date, an electron transfer phenomenon is commonly found in the Hg^{2+} sensing system. Hg^{2+} strongly binds to Au^{0}. Subsequently, energy transfer takes place as the excited electron of Au is transferred to Hg^{2+}.[35] Besides Hg^{2+} sensing, the fluorescence quenching can occur *via* aggregation of AuNCs. Metal ions such as Fe^{3+}, Cu^{2+}, and Pb^{2+} can strongly coordinate to the ligands on the adjacent AuNCs, inducing aggregation, thereby attenuating the fluorescence.[28-30, 32]

In this study, we introduced fluorescent AuNCs comprising tyrosine-containing tripeptides, tyrosine-cysteine-tyrosine (YCY) and serine-cysteine-tyrosine (SCY). A cysteine residue was employed to utilize thiol functional group for Au-S bonding. For SCY, tyrosine residue at the N-terminus of the YCY was replaced with serine to examine the impact of the number of tyrosine residues. Blue and red fluorescence-emitting AuNCs from the YCY peptide (Blue-YCY-AuNC and Red-YCY-AuNC, respectively hereafter) and blue fluorescence-emitting SCY-AuNC (Blue-SCY-AuNC hereafter) were obtained. Subsequently, we investigated the metal ions sensing ability of these AuNCs. We found that Fe^{3+} and Cu^{2+} can effectively suppress fluorescence emission of AuNCs while other metal

ions at the same concentration did not cause any quenching. We propose a plausible mechanism in which chelation between the peptide on the AuNC surface and the target ions results in aggregation and causes fluorescence quenching.

Experimental section

Materials

N,N-Dimethylformamide (DMF), methanol (MeOH), acetonitrile (ACN), dimethyl sulfoxide (DMSO), ethyl ether and dichloromethane (DCM) were purchased from Thermo Fisher Scientific. Trifluoroacetic acid (TFA), 5,5′-dithiobis(2-nitrobenzoic acid) (DTNB), glutathione (GSH), *N,N*-diisopropylethylamine (DIPEA), and piperidine were obtained from Sigma-Aldrich. Nitrate salts of metal ions ($AgNO_3$, $Al(NO_3)_3$, $Ba(NO_3)_2$, $Ca(NO_3)_2$, $Co(NO_3)_2$. $Cu(NO_3)_2$, $Fe(NO_3)_3$, KNO_3, $Mg(NO3)_2$, $NaNO_3$, $Ni(NO_3)_2$, $Pb(NO_3)_2$, and $Zn(NO_3)_2$) were purchased from Sigma-Aldrich. Auric chloride ($HAuCl_4 \cdot 3H_2O$) was obtained from Sigma-Aldrich. Fmoc-Tyr(tBu)-OH, Fmoc-Cys(Trt)-OH, Fmoc-Ser(tBu)-OH, Rink Amide MBHA resin (100-200 mesh) and 2-(1H-benzotriazol-1-yl)-1,1,3,3-tetramethyluronium hexfluorophosphate (HBTU) were purchased from Novabiochem. 1-Hydroxybenzotriazole hydrate ($HOBt \cdot H_2O$) was obtained from Creosalus. Sephadex™ G-25 was purchased from GE Healthcare. Dialysis membrane kit (Slide-A-Lyzer® Dialysis Cassette G2; 3.5 kDa cutoff) was obtained from Thermo Scientific. Ultrapure water (18.2 MΩcm, Millipore Co.) was used in all experiments.

Synthesis of tripeptides

Tyrosine-cysteine-tyrosine (YCY) and serine-cysteine-tyrosine (SCY) peptides were synthesized using Rink Amide MBHA resins. 600 mg of Rink Amide MBHA resins was swelled in 3 mL of DMF for 1 h. Fmoc deprotection was achieved with 20% piperidine (20% in DMF v/v). After washing 5 times with DMF, 2 times with MeOH, 2 times with DCM, and 3 times with DMF, a solution of 5 equivalents of Fmoc-Tyr(*t*Bu)-OH, $HOBt \cdot H_2O$, HBTU, and 10 equivalents of DIPEA in dry DMF was added to the resins and mixed at room temperature for 3 h. All the resins were fully washed after each reaction step. The resins were

treated with 20% piperidine for Fmoc deprotection and were mixed with a solution of Fmoc-Cys(Trt)-OH (5 eq.), HOBt·H_2O (5 eq.), HBTU (5 eq.), and DIPEA (10 eq.) in dry DMF for 3 h. After Fmoc deprotection with 20% piperidine, the beads were divided equally into 2 fritted syringes. One syringe was mixed with a solution of Fmoc-Tyr(*t*Bu)-OH (5 eq.), HOBt·H_2O (5 eq.), HBTU (5 eq.), and DIPEA (10 eq.) in dry DMF for 3 h. The other syringe was mixed with Fmoc-Ser(tBu)-OH (5 eq.), HOBt·H_2O (5 eq.), HBTU (5 eq.), and DIPEA (10 eq.) in dry DMF. After the peptide coupling reaction, the Fmoc protecting group was removed with 20% piperidine. The peptides were cleaved and deprotected in a TFA cocktail solution (95% TFA, 2.5% TIS, 2.5% H_2O) for 2 h and additional 20 min with the fresh TFA cocktail solution. The solution was collected and evaporated under argon gas. When the volume of the solution was at 10% of the initial volume, chilled ethyl ether was added to the solution. The resulting solution was centrifuged at 4,000 g and the supernatant was discarded. This step was repeated two times more. The precipitates were dried under vacuum. The resulting powders were dissolved in water with 0.1% TFA and purified by preparative RP-HPLC. Pure fractions were identified by HPLC-MS/MS (HPLC: Agilent, 1100 Series, MS/MS: Sciex, 4000 Q Trap). After purification, purity of the tripeptides was evaluated by analytical HPLC-MS/MS. The combined pure fractions were lyophilized and kept at -20 °C before use.

Preparation of YCY- and SCY-templated fluorescent AuNCs

The concentration of the YCY- and SCY aqueous solutions was determined by Ellman's reagent (DTNB). Glutathione was used as a standard reagent. The glass vial was cleaned using Aqua regia (HCl: HNO_3, 3:1 v/v) and thoroughly rinsed with H_2O prior to use. In the typical method for the synthesis of peptide templated AuNCs, 0.5 mL of peptide solution (25 mM in H_2O) was slowly added to 0.5 mL of $HAuCl_4 \cdot 3H_2O$ (25 mM in H_2O) with stirring. After mixing the solution for 15 min at 70 °C, the pH of the solution was adjusted to pH 10 with 1M NaOH solution. The mixed solution was then kept stirring at 70 °C for 8 h. The solution was cooled to the room temperature, transferred to 1.5 mL individual microtubes and centrifuged at 16,000 g for 10 min to remove the sediment and other

impurities. The Blue-YCY-AuNCs and Blue-SCY-AuNCs were in the supernatant and the Red-YCY-AuNCs were trapped inside of the precipitates after centrifugation. The Red-YCY-AuNCs were extracted by 1:1 of DMSO and 10% acetic acid aqueous solution. After 10 min sonication, the solution was centrifugated at 16,000 g for 30 min to remove the precipitates. The yellow clear supernatants were transferred into new tubes. Each AuNC solutions was purified *via* a Sephadex^{TM} G-25 column equilibrated and eluted with H_2O (1 mL/min). Fractions of eluate (0.5 mL) were collected and analyzed by a UV-Vis absorption and fluorescence spectroscopy using a microplate reader. Fractions containing fluorescent AuNC were collected and dialyzed in H_2O using a 3.5 kDa cutoff membrane to separate the AuNCs from any unreacted species and to adjust pH to be a neutral. The AuNC suspensions were stored at 4 °C in dark for further characterization and experiment.

Characterization of AuNCs

UV-Vis spectra of the AuNC solution were measured with a microplate reader (Spark 20M; Tecan). Fluorescence spectra were obtained with Horiba Fluorolog fluorometer (Horiba Scientific). The measurement was conducted with 1 cm quartz cuvette at the room temperature. The slits for the excitation and the emission were set to 5 nm. TEM images were taken using the JEM-2100F (JEOL). A drop of the AuNC solution (0.1 mg/mL) was deposited on a carbon-coated Cu grid and analyzed. Dynamic light scattering (DLS) and zeta-potential were measured by Nano-ZS (Malvern Instrument).

The influence of pH and NaCl on fluorescence intensity

The pH and the salt sensitivity of the AuNC were characterized by mixing 100 μL of each AuNC solution (Blue-YCY-AuNC and Blue-SCY-AuNC: 0.5 mg/mL, Red-YCY-AuNC: 0.15 mg/mL) with 400 μL of the different buffer solutions and NaCl solutions. The fluorescence emission spectra were obtained with 325 nm excitation and 400 nm excitation for blue fluorescence-emitting and red fluorescence-emitting AuNC, respectively.

Fluorescent detections of metal ions

The following metal salts were used: Ag^{+}, Al^{3+}, Ba^{2+}, Ca^{2+}, Co^{2+}, Cu^{2+}, Fe^{3+}, K^{+}, Mg^{2+}, Na^{+}, Ni^{2+}, Pb^{2+}, and Zn^{2+}. These metal salts were dissolved in H_2O. 300 μL of each AuNC solution (Blue-YCY-AuNC and Blue-SCY-AuNC: 0.2 mg/mL, Red-YCY-AuNC: 0.06 mg/mL) and 300 μL of each metal ion solution (100 μM) were mixed and the mixture was left to be equilibrated at the room temperature for 2 min. 500 μL of the solution was placed in the cuvette and the fluorescence quenching spectra were measured from appropriate excitation wavelength (Blue-YCY-AuNC and Blue-SCY-AuNC: 325 nm, Red-YCY-AuNC: 400 nm). Serial dilutions of Fe^{3+} and Cu^{2+} were also mixed with each AuNC solution and incubated for 2 min before the measurement.

Quantum yield (QY) measurement of AuNCs

Quantum yields of each AuNC were calculated using the formula, $\Phi_X = \Phi_{ST}\left(\frac{Grad_X}{Grad_{ST}}\right)\left(\frac{\eta^2_X}{\eta^2_{ST}}\right)$,

where the subscripts ST and X denote standard and sample respectively, Φ is the fluorescence quantum yield, Grad the gradient from the plot of integrated fluorescence intensity versus absorbance, and η is the refractive index of the solvent. We used quinine sulfate (QY: 0.54) in 0.1 M H_2SO_4 (η: 1.33) as a fluorescence standard for the calculation of the QY of Blue-YCY- and Blue-SCY-AuNCs. For the measurement of the QY of Red-YCY-AuNC, 9,10-diphenyl anthracene (QY: 0.90) in cyclohexane (η: 1.44) was used as a reference fluorophore. We recorded the UV-vis absorbance spectrum of five serial solutions of each sample including solvent background for the chosen references. Afterward, the fluorescence spectra of the same solution in the 1 cm fluorescence cuvette were measured. Graphs of integrated fluorescence intensity versus absorbance were plotted.

Results and discussion

Preparation of AuNCs

In this study, we synthesized fluorescent AuNCs by employing tyrosine-containing tripeptide as both a reducing agent and stabilizer (Scheme 1). Under alkaline conditions, the

phenolate group in tyrosine was expected to reduce Au^{3+} to Au^{0} through electron transfer resulting in the formation of a semi-quinone.[29, 36] We increased the temperature to accelerate the reduction of Au^{3+} ions. The important condition in utilizing the reduction capability of tyrosine for the synthesis of AuNC is pH.[19, 37] In order to optimize pH condition for synthesizing peptide-templated AuNCs, we added different amounts of 1 M NaOH to the mixture of $HAuCl_4$ and the peptide. The purity of the synthesized peptides was shown in Figures S1. Glutathione was used as a control peptide as it has been used to synthesize fluorescent AuNC.[32, 38] After 8 h reaction at 70 °C, the strong fluorescent emission peak at 415 nm for both of YCY- and SCY-AuNCs appeared with 325 nm excitation when the pH of the mixture was greater than 7 (Figures 1 a and c). The strongest emission peak of YCY- and SCY-AuNCs was achieved at pH 10. Interestingly, an additional emission peak from YCY-AuNC was observed at 670 nm from 400 nm excitation (Figure 1d), but not from the SCY-AuNC. Under the acidic and neutral pH conditions, on the other hand, the GSH-AuNC gave fluorescence spectra with two distinct peaks at 390 nm and 800 nm from 325 nm excitation and with a peak at 800 nm from 400 nm excitation (Figures 1e and f). From this result, we found that the optimal pH condition for the synthesis of fluorescent AuNCs was pH 10, in which the tyrosine further facilitated the formation of AuNCs. Under the optimal condition, the color of YCY solution changed from colorless to red, and the color of SCY solution changed from colorless to brown during the reaction. The solutions of YCY- and SCY-AuNC were centrifuged to remove the sediment and agglomerated particles. The strong blue emission was observed under the 365 nm UV lamp in the supernatants of YCY- and SCY-AuNC solutions. Interestingly, the precipitates of the centrifuged YCY-AuNC solution emitted deep-red fluorescence under the 365 nm UV lamp. We obtained red-emitting YCY-AuNCs from the precipitates using 10% acetic acid and DMSO (1:1 v/v). Afterward, we purified AuNCs by a size exclusion chromatography to remove unreacted peptides, Au ions, and non-fluorescent gold nanoparticles, which were not removed by the centrifugation (Figure S2). After the dialysis, the AuNC solutions exhibited neutral pH (~ pH 7).

The optical and physical characteristics of the AuNCs.

Images in Figure 2 are Blue-YCY-AuNC, Blue-SCY-AuNC, and Red-YCY-AuNC under 365nm UV lamp showing uniform dispersity of the AuNCs in aqueous solution with slight yellow color under the visible light. In the UV-vis spectra (Figures 2, blue curves), the absence of surface plasmon resonance peak (520-530 nm) indicates that the synthesized AuNCs were smaller than 2.5 nm in diameter.[39] A distinct peak at 325 nm appeared in the UV-Vis absorption spectra of Blue-YCY-AuNC and Blue-SCY-AuNC. The strong blue emission wavelength (415 nm) of Blue-YCY-AuNC and Blue-SCY-AuNC was achieved when excited at 325 nm (Figures 2b and c). The emission peak of Red-YCY-AuNC appeared at 670 nm (Figure 2a). Fluorescence quantum yields of Red-YCY-AuNC, Blue-YCY-AuNC, and Blue-SCY-AuNC are 0.8%, 1.2%, and 1.5%, respectively.

High resolution TEM images indicate that all the peptide-templated AuNCs were monodispersed with uniformity in size and spherical shape (Figures 3a, d, and g). Size distribution histograms of each peptide-templated AuNCs were constructed by measuring diameters of 100 individual AuNCs (Figures 3b, e, and h). The average size of the Blue-SCY-AuNC was found to be 1.7 ± 0.3 nm. Interestingly, Blue- and Red-YCY-AuNCs exhibited almost identical size, 1.8 ± 0.5 nm and 1.8 ± 0.3 nm, respectively. However, according to DLS results, hydrodynamic diameters of all peptide-templated AuNCs were larger than those obtained from TEM analysis (Figures 3c, f and i). This discrepancy can be explained by the external immobilization and the hydration of peptides on nanoclusters. Taken together, these experimental results demonstrate that we have successfully prepared fluorescent peptide templated AuNCs without requiring any additional chemical reducing agents.

As shown in Figure 4a, all AuNCs were stable under high ionic strength conditions. To investigate the fluorescent response of the AuNCs to pH changes, we measured fluorescence intensities of the AuNCs after mixing with buffer solutions with different pH. As shown in Figure 4 b (red circle and blue triangle,) fluorescence intensities of blue-YCY- and SCY-AuNCs decreased from pH 7 to pH 4. On the contrary, under the alkaline conditions the fluorescence of the AuNCs showed increase in the emission. Interestingly, Red-YCY-AuNCs exhibited the complete opposite trend of blue-emitting AuNCs (Figure 4b, black

square). We speculate that the YCY and SCY peptides on the surface of Blue-YCY-AuNC and Blue-SCY-AuNC may have the same surface configurations to Au atoms while the configuration of Red-YCY-AuNC is different. This notion can be supported by the results of zeta potential measurement of each AuNC. Blue-YCY- and SCY-AuNCs exhibited -13.0 mV and -11.8 mV in H_2O at the room temperature, while Red-YCY-AuNC exhibited +45.6 mV. It is possible that the YCY of Red-YCY-AuNC may adopt a configuration in which O^- group of the unoxidized tyrosine and -SH of the cysteine form coordination bonds to Au atoms resulting in strongly positive charge in zeta potential for Red-YCY-AuNC.[40] In the case of blue-emitting AuNCs, the coordination bond only involves the -SH of the cysteine and the Au atoms, causing weakly negative charge in blue fluorescence-emitting AuNCs.

Metal selectivity and sensitivity of AuNCs

Tyrosine residue in the peptide is known to show a strong interaction with the transition metal ion by forming a square planar complex in which the C-terminal carboxylate, amide nitrogen, and N-terminal amine bind to metal ions.[40, 41] In addition, studies have suggested that the oxidized form of tyrosine side chain, a semi-quinone, that are produced when Au^{3+} is reduced to Au^0, may form complexes with Fe^{3+} and Cu^{2+}.[42, 43] Therefore, we explored the sensing capability of the synthesized AuNCs to various metal ions. We mixed the same volume of the AuNC solution and 13 different metal ion solutions (100 μM) and measured fluorescence intensities. As shown in Figure 5a, a significant fluorescence quenching (~85%) of Blue-YCY-AuNC was found in the presence of 50 μM Fe^{3+}, and a 75% fluorescence quenching of Blue-SCY-AuNC was observed compared to the blank sample (Figure 5b). Furthermore, Blue-YCY- and SCY-AuNCs responded to Cu^{2+} and Al^{3+} with ~75% and ~45% quenching efficiency, respectively (Figures 5a and b). On the other hand, Ag^+, Ba^{2+}, Ca^{2+}, Co^{2+}, K^+, Mg^{2+}, Na^+, Ni^+, Pb^{2+}, and Zn^{2+} ions did not significantly affect fluorescence signals of Blue-YCY- and SCY-AuNCs. Interestingly, the fluorescence signals of Red-YCY-AuNCs are stable for all 13 different metal ions (Figure 5d). Since both blue fluorescence-emitting AuNCs are more sensitive to Fe^{3+} and Cu^{2+}, we further evaluated the interaction between blue fluorescence-emitting AuNCs and the two metal ions. We

monitored changes in fluorescence under various concentrations of Fe^{3+} and Cu^{2+}. The fluorescence quenching data was fitted to the Stern-Volmer equation:[42, 44]

$$F_0/F = 1 + K_{sv}[Q],$$

where K_{sv} is the Stern-Volmer quenching constant, [Q] is the analyte quenchers (Fe^{3+} or Cu^{2+}), and F_0 and F are the fluorescence intensities of the AuNCs at 415 nm in the absence and presence of metal ions. As observed in Figure 6a, the intensities of the fluorescence emission at 415 nm, in general, gradually decreased as the concentrations of Fe^{3+} and Cu^{2+} increased, up to approximately 40 μM when the emission begins to plateau (summarized in Table 1). Blue-YCY-AuNC for Fe^{3+} sensing, on the other hands, did not exhibit this plateau trend. Fluorescence intensity continued to decrease with Fe^{3+} and Cu^{2+} concentration, with a strong linear correlation R^2 of 0.995 and 0.997 at concentrations ranging from 0.25 μM to 100 μM and from 0.25 μM to 25 μM, respectively (Figure 6b). In addition, the Blue-SCY-AuNC also has a strong linear relationship with Fe^{3+} (R^2=0.965) and Cu^{2+} (R^2=0.993) from 0.25 μM to 37.5 μM and from 0.25 μM to 25 μM, respectively. Furthermore, Blue-YCY-AuNC exhibits higher sensitivity to Fe^{3+} and Cu^{2+} than the Blue-SCY-AuNC (Table 1), possibly due to the additional tyrosine residue in Blue-YCY-AuNC. The limit of detection (LOD) was calculated from the slope of the plot of the Stern-Volmer equation versus concentrations of Fe^{3+} and Cu^{2+}. The LOD value was calculated according to the assumption of LOD equal to 3SD/S, where SD represents standard deviation of intercept and S represents the slope of linear curve.[32] We obtained 3.2 μM and 0.77 μM of LOD values for Blue-YCY-AuNC on sensing for Fe^{3+} and Cu^{2+}, respectively. The LODs for Blue-SCY-AuNC are 4.1 μM and 1.3 μM for sensing of Fe^{3+} and Cu^{2+}. Therefore, two-tyrosine containing peptide (YCY)-templated AuNC has better optical sensor ability toward to Fe^{3+} and Cu^{2+}.

Sensing mechanism

According to previous reports, ligands containing tyrosine or oxidized tyrosine can chelate metals such as Fe^{3+} and Cu^{2+} ions.[40, 43, 45] We examined the sensing mechanism by monitoring the hydrodynamic diameter of AuNCs after adding Fe^{3+} and Cu^{2+} to AuNC solutions. We also tested Ni^{2+} as a comparison to examine if the aggregation of AuNCs would

occur in the presence of some specific target ions. The size-distribution histogram of each AuNC with Fe^{3+} and Cu^{2+} in Figure 7 revealed that the Blue-YCY-AuNC exceptionally tended to aggregate in the presence of Fe^{3+} ions, resulting in the formation of huge agglomerates (hydrodynamic diameter ~1,200 nm). Similarly, when the Blue-YCY-AuNC was mixed with Cu^{2+}, they formulated ~25 nm complexes, smaller than the complexes form from the Blue-YCY-AuNC and Fe^{3+} (Figure 7a). The results strongly correlate with the tendency of the quenching efficiency of the Blue-YCY-AuNC towards Fe^{3+} and Cu^{2+} (Figure 5d). Under the identical circumstance, Fe^{3+} and Cu^{2+} induced the aggregation of Blue-SCY-AuNC forming ~33 nm and ~12 nm complexes, respectively (Figure 7b). However, there is no significant aggregation in the presence of Ni^{2+} in both of Blue-YCY- and SCY-AuNCs. In addition to these results, the DLS histogram of the Red-YCY-AuNC exhibits no aggregation even in the presence of Fe^{3+} and Cu^{2+} (Figure 7c). The results of DLS measurement have provided further evidence that the peptides on blue fluorescence-emitting AuNCs and Red-YCY-AuNC have different binding configuration to Au atoms. In case of YCY on the Red-YCY-AuNC, as we proposed above, all the side chains functional groups are bound to Au atom. Therefore, no functional groups are available to chelate to metal ions. In contrast, for YCY and SCY peptides on Blue-YCY- and SCY-AuNC, only cysteine side chain -SH is bound to Au atoms. Therefore, the semi-quinone of the oxidized tyrosine and the N-terminal NH_2 group can form complexes with Fe^{3+} and Cu^{2+}, resulting in aggregation-induced fluorescence quenching.[29,45,46] These findings indicate that semi-quinones on the surface of AuNCs create aggregation by forming complexes with the other ligands of adjacent AuNCs. In addition, based on the DLS results, the aggregation propensity, and therefore the sensing capacity, of AuNC strongly correlates with the number of possible semi-quinones on AuNCs.

Conclusion

In summary, by employing tyrosine-containing tripeptides, we successfully synthesized fluorescent AuNCs with emission wavelength 415 nm and 670 nm without using additional reducing agents. The as-prepared AuNCs displayed ultrasmall size (< 2.5 nm),

mono-dispersity, and uniform spherical shape in TEM images and DLS analyses. When the Blue-YCY-AuNC and Blue-SCY-AuNC were used to probe 13 metal ions, only Fe^{3+} and Cu^{2+} ions showed a significant fluorescence quenching of AuNCs. On the contrary, Red-YCY-AuNC displayed stable fluorescence signal in the presence of 13 metal ions. The Blue-YCY-AuNC showed higher sensitivity and a wider sensing range of Fe^{3+} and Cu^{2+} than the Blue-SCY-AuNC, with a lower detection limit of 3.2 μM and 0.77 μM, respectively. The interaction mechanism and sensing performance of AuNCs were systematically investigated using fluorescence spectra and DLS. In accordance with the fluorescence response of AuNCs to metal ions, the Fe^{3+} induced the aggregation of Blue-YCY-AuNC and formed larger complexes compared to the complexes formed with Cu^{2+}. Furthermore, the Blue-SCY-AuNC induced aggregation in the presence of Fe^{3+} and Cu^{2+}, though these complexes are smaller than those of Blue-YCY-AuNC. Overall, although the number of tyrosine residue may not have a significant impact on the formation of AuNCs, the number oxidized tyrosine (semi-quinone form) on the surface of AuNC may play a critical role in the detection of target metal ions. This study provides a new and facile strategy to design surface ligands for AuNC to sense metal ions.

Acknowledgement

This work was funded in part by a grant from the Welch Foundation (BP-0037).

References

1. Fang, J.; Li, J.; Zhang, B.; Yuan, X.; Asakura, H.; Tanaka, T.; Teramura, K.; Xie, J.; Yan, N., The support effect on the size and catalytic activity of thiolated Au(2)(5) nanoclusters as precatalysts. *Nanoscale* **2015,** *7* (14), 6325-33.
2. Yahia-Ammar, A.; Sierra, D.; Merola, F.; Hildebrandt, N.; Le Guevel, X., Self-Assembled Gold Nanoclusters for Bright Fluorescence Imaging and Enhanced Drug Delivery. *ACS Nano* **2016,** *10* (2), 2591-9.
3. Ju, E.; Liu, Z.; Du, Y.; Tao, Y.; Ren, J.; Qu, X., Heterogeneous assembled nanocomplexes for ratiometric detection of highly reactive oxygen species in vitro and in vivo. *ACS Nano* **2014,** *8* (6), 6014-23.
4. Zhang, C.; Li, C.; Liu, Y.; Zhang, J.; Bao, C.; Liang, S.; Wang, Q.; Yang, Y.; Fu, H.; Wang, K.; Cui, D., Gold Nanoclusters-Based Nanoprobes for Simultaneous Fluorescence Imaging and Targeted Photodynamic Therapy with Superior Penetration and Retention Behavior in Tumors. *Advanced Functional Materials* **2015,** *25* (8), 1314-1325.
5. Sun, S.; Ning, X.; Zhang, G.; Wang, Y. C.; Peng, C.; Zheng, J., Dimerization of Organic Dyes on Luminescent Gold Nanoparticles for Ratiometric pH Sensing. *Angew Chem Int Ed Engl* **2016,** *55* (7), 2421-4.
6. Zhang, X.; Chen, X.; Jiang, Y. W.; Ma, N.; Xia, L. Y.; Cheng, X.; Jia, H. R.; Liu, P.; Gu, N.; Chen, Z.; Wu, F. G., Glutathione-Depleting Gold Nanoclusters for Enhanced Cancer Radiotherapy through Synergistic External and Internal Regulations. *ACS Appl Mater Interfaces* **2018,** *10* (13), 10601-10606.
7. Zheng, K.; Setyawati, M. I.; Leong, D. T.; Xie, J., Antimicrobial Gold Nanoclusters. *ACS Nano* **2017,** *11* (7), 6904-6910.
8. Lee, T. H.; Gonzalez, J. I.; Zheng, J.; Dickson, R. M., Single-molecule optoelectronics. *Acc Chem Res* **2005,** *38* (7), 534-41.
9. Zheng, J.; Nicovich, P. R.; Dickson, R. M., Highly fluorescent noble-metal quantum dots. *Annu Rev Phys Chem* **2007,** *58*, 409-31.
10. El-Sayed, M. A., Some interesting properties of metals confined in time and nanometer space of different shapes. *Acc Chem Res* **2001,** *34* (4), 257-64.
11. Jin, R., Quantum sized, thiolate-protected gold nanoclusters. *Nanoscale* **2010,** *2* (3), 343-62.
12. Gui, Y.; Wang, Y.; He, C.; Tan, Z.; Gao, L.; Li, W.; Bi, H., Multi-optical signal channel gold nanoclusters and their application in heavy metal ions sensing arrays. *Journal of Materials Chemistry C* **2021,** *9* (8), 2833-2839.
13. Burratti, L.; Ciotta, E.; Bolli, E.; Kaciulis, S.; Casalboni, M.; De Matteis, F.; Garzón-Manjón, A.; Scheu, C.; Pizzoferrato, R.; Prosposito, P., Fluorescence enhancement induced by the interaction of silver nanoclusters with lead ions in water. *Colloids and Surfaces A: Physicochemical and Engineering Aspects* **2019,** *579*, 123634.
14. Luo, P.; Zheng, Y.; Qin, Z.; Li, C.; Jiang, H.; Wang, X., Fluorescence light up detection of aluminium ion and imaging in live cells based on the aggregation-induced emission enhancement of thiolated gold nanoclusters. *Talanta* **2019,** *204*, 548-554.

15. Nain, A.; Tseng, Y.-T.; Lin, Y.-S.; Wei, S.-C.; Mandal, R. P.; Unnikrishnan, B.; Huang, C.-C.; Tseng, F.-G.; Chang, H.-T., Tuning the photoluminescence of metal nanoclusters for selective detection of multiple heavy metal ions. *Sensors and Actuators B: Chemical* **2020,** *321*, 128539.
16. Duan, H.; Nie, S., Etching colloidal gold nanocrystals with hyperbranched and multivalent polymers: a new route to fluorescent and water-soluble atomic clusters. *J Am Chem Soc* **2007,** *129* (9), 2412-3.
17. Lin, C. A.; Yang, T. Y.; Lee, C. H.; Huang, S. H.; Sperling, R. A.; Zanella, M.; Li, J. K.; Shen, J. L.; Wang, H. H.; Yeh, H. I.; Parak, W. J.; Chang, W. H., Synthesis, characterization, and bioconjugation of fluorescent gold nanoclusters toward biological labeling applications. *ACS Nano* **2009,** *3* (2), 395-401.
18. Chen, T.-H.; Nieh, C.-C.; Shih, Y.-C.; Ke, C.-Y.; Tseng, W.-L., Hydroxyl radical-induced etching of glutathione-capped gold nanoparticles to oligomeric AuI–thiolate complexes. *RSC Advances* **2015,** *5* (56), 45158-45164.
19. Song, W.; Liang, R. P.; Wang, Y.; Zhang, L.; Qiu, J. D., Green synthesis of peptide-templated gold nanoclusters as novel fluorescence probes for detecting protein kinase activity. *Chem Commun (Camb)* **2015,** *51* (49), 10006-9.
20. Chakraborty, S.; Babanova, S.; Rocha, R. C.; Desireddy, A.; Artyushkova, K.; Boncella, A. E.; Atanassov, P.; Martinez, J. S., A Hybrid DNA-Templated Gold Nanocluster For Enhanced Enzymatic Reduction of Oxygen. *J Am Chem Soc* **2015,** *137* (36), 11678-87.
21. Li, H.; Huang, H.; Feng, J.-J.; Luo, X.; Fang, K.-M.; Wang, Z.-G.; Wang, A.-J., A polypeptide-mediated synthesis of green fluorescent gold nanoclusters for Fe3+ sensing and bioimaging. *Journal of Colloid and Interface Science* **2017,** *506*, 386-392.
22. Duan, Y.; Duan, R.; Liu, R.; Guan, M.; Chen, W.; Ma, J.; Chen, M.; Du, B.; Zhang, Q., Chitosan-Stabilized Self-Assembled Fluorescent Gold Nanoclusters for Cell Imaging and Biodistribution in Vivo. *ACS Biomater Sci Eng* **2018,** *4* (3), 1055-1063.
23. Yang, L.; Wang, H.; Li, D.; Li, L.; Lou, X.; Liu, H., Self-Nucleation and Self-Assembly of Highly Fluorescent Au5 Nanoclusters for Bioimaging. *Chemistry of Materials* **2018,** *30* (15), 5507-5515.
24. Nandi, I.; Chall, S.; Chowdhury, S.; Mitra, T.; Roy, S. S.; Chattopadhyay, K., Protein Fibril-Templated Biomimetic Synthesis of Highly Fluorescent Gold Nanoclusters and Their Applications in Cysteine Sensing. *ACS Omega* **2018,** *3* (7), 7703-7714.
25. Zhang, N.; Si, Y.; Sun, Z.; Chen, L.; Li, R.; Qiao, Y.; Wang, H., Rapid, Selective, and Ultrasensitive Fluorimetric Analysis of Mercury and Copper Levels in Blood Using Bimetallic Gold–Silver Nanoclusters with "Silver Effect"-Enhanced Red Fluorescence. *Analytical Chemistry* **2014,** *86* (23), 11714-11721.
26. Chen, T.-H.; Tseng, W.-L., (Lysozyme Type VI)-Stabilized Au8 Clusters: Synthesis Mechanism and Application for Sensing of Glutathione in a Single Drop of Blood. *Small* **2012,** *8* (12), 1912-1919.
27. Xie, J.; Zheng, Y.; Ying, J. Y., Protein-directed synthesis of highly fluorescent gold nanoclusters. *J Am Chem Soc* **2009,** *131* (3), 888-9.

28. Zhang, J.; Cai, C.; Razzaque, S.; Hussain, I.; Lu, Q.-W.; Tan, B., Synthesis of water-soluble and highly fluorescent gold nanoclusters for Fe3+ sensing in living cells using fluorescence imaging. *Journal of Materials Chemistry B* **2017,** *5* (28), 5608-5615.
29. Annie Ho, J.-a.; Chang, H.-C.; Su, W.-T., DOPA-Mediated Reduction Allows the Facile Synthesis of Fluorescent Gold Nanoclusters for Use as Sensing Probes for Ferric Ions. *Analytical Chemistry* **2012,** *84* (7), 3246-3253.
30. Bothra, S.; Upadhyay, Y.; Kumar, R.; Ashok Kumar, S. K.; Sahoo, S. K., Chemically modified cellulose strips with pyridoxal conjugated red fluorescent gold nanoclusters for nanomolar detection of mercuric ions. *Biosensors and Bioelectronics* **2017,** *90*, 329-335.
31. Wang, J.; Ma, S.; Ren, J.; Yang, J.; Qu, Y.; Ding, D.; Zhang, M.; Yang, G., Fluorescence enhancement of cysteine-rich protein-templated gold nanoclusters using silver(I) ions and its sensing application for mercury(II). *Sensors and Actuators B: Chemical* **2018,** *267*, 342-350.
32. Bain, D.; Maity, S.; Paramanik, B.; Patra, A., Core-Size Dependent Fluorescent Gold Nanoclusters and Ultrasensitive Detection of Pb2+ Ion. *ACS Sustainable Chemistry & Engineering* **2018,** *6* (2), 2334-2343.
33. Deng, L.; Zhou, Z.; Li, J.; Li, T.; Dong, S., Fluorescent silver nanoclusters in hybridized DNA duplexes for the turn-on detection of Hg2+ ions. *Chemical Communications* **2011,** *47* (39), 11065-11067.
34. Zhao, Q.; Chen, S.; Zhang, L.; Huang, H.; Zeng, Y.; Liu, F., Multiplex sensor for detection of different metal ions based on on–off of fluorescent gold nanoclusters. *Analytica Chimica Acta* **2014,** *852*, 236-243.
35. Xie, J.; Zheng, Y.; Ying, J. Y., Highly selective and ultrasensitive detection of Hg2+ based on fluorescence quenching of Au nanoclusters by Hg2+–Au+ interactions. *Chemical Communications* **2010,** *46* (6), 961-963.
36. Selvakannan, P. R.; Swami, A.; Srisathiyanarayanan, D.; Shirude, P. S.; Pasricha, R.; Mandale, A. B.; Sastry, M., Synthesis of Aqueous Au Core−Ag Shell Nanoparticles Using Tyrosine as a pH-Dependent Reducing Agent and Assembling Phase-Transferred Silver Nanoparticles at the Air−Water Interface. *Langmuir* **2004,** *20* (18), 7825-7836.
37. Wang, Y.; Cui, Y.; Zhao, Y.; Liu, R.; Sun, Z.; Li, W.; Gao, X., Bifunctional peptides that precisely biomineralize Au clusters and specifically stain cell nuclei. *Chemical Communications* **2012,** *48* (6), 871-873.
38. Zhang, G.-m.; Li, Y.; Xu, J.; Zhang, C.; Shuang, S.; Dong, C.; Choi, M. M. F., Glutathione-protected fluorescent gold nanoclusters for sensitive and selective detection of Cu2+. *Sensors and Actuators B-chemical* **2013,** *183*, 583-588.
39. Vasimalai, N.; Fernández-Argüelles, M. T.; Espiña, B., Detection of Sulfide Using Mercapto Tetrazine-Protected Fluorescent Gold Nanodots: Preparation of Paper-Based Testing Kit for On-Site Monitoring. *ACS Applied Materials & Interfaces* **2018,** *10* (2), 1634-1645.
40. Contino, A.; Maccarrone, G.; Zimbone, M.; Reitano, R.; Musumeci, P.; Calcagno, L.; Oliveri, I. P., Tyrosine capped silver nanoparticles: A new fluorescent sensor for the quantitative determination of copper(II) and cobalt(II) ions. *Journal of Colloid and Interface Science* **2016,** *462*, 216-222.

41. Pettit, L. D.; Steel, I.; Kowalik, T.; Kozlowski, H.; Bataille, M., Specific binding of the tyrosine residue in copper(II) complexes of Tyr-Pro-Gly-Tyr and Tyr-Gly-Pro-Tyr. *Journal of the Chemical Society, Dalton Transactions* **1985,** (6), 1201-1205.
42. Lu, W.; Qin, X.; Liu, S.; Chang, G.; Zhang, Y.; Luo, Y.; Asiri, A. M.; Al-Youbi, A. O.; Sun, X., Economical, Green Synthesis of Fluorescent Carbon Nanoparticles and Their Use as Probes for Sensitive and Selective Detection of Mercury(II) Ions. *Analytical Chemistry* **2012,** *84* (12), 5351-5357.
43. Gordon, D. J.; Fenske, R. F., Theoretical study of o-quinone complexes of iron. *Inorganic Chemistry* **1982,** *21*, 2916-2923.
44. Liu, Y.; Ai, K.; Cheng, X.; Huo, L.; Lu, L., Gold-Nanocluster-Based Fluorescent Sensors for Highly Sensitive and Selective Detection of Cyanide in Water. *Advanced Functional Materials* **2010,** *20* (6), 951-956.
45. Dikalov, S. I.; Rumyantseva, G. V.; Piskunov, A. V.; Weiner, L. M., Role of quinone-iron(III) interaction in NADPH-dependent enzymatic generation of hydroxyl radicals. *Biochemistry* **1992,** *31* (37), 8947-53.

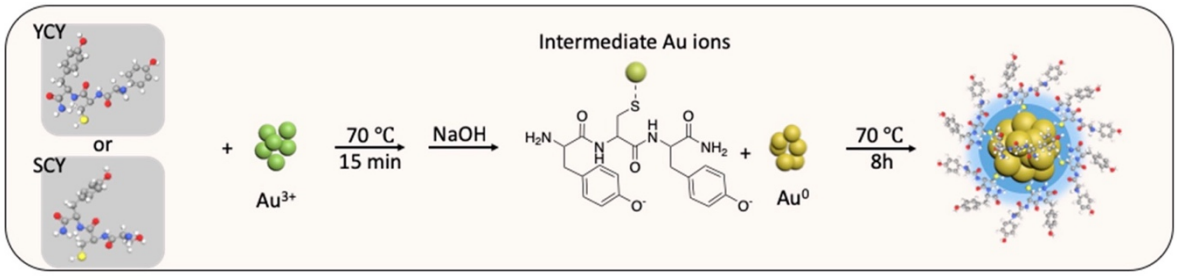

Scheme 1. Schematic illustration of the preparation of fluorescent AuNC *via* tyrosine-assisted reduction. Intermediate Au ions with SCY peptide was not shown for simplicity.

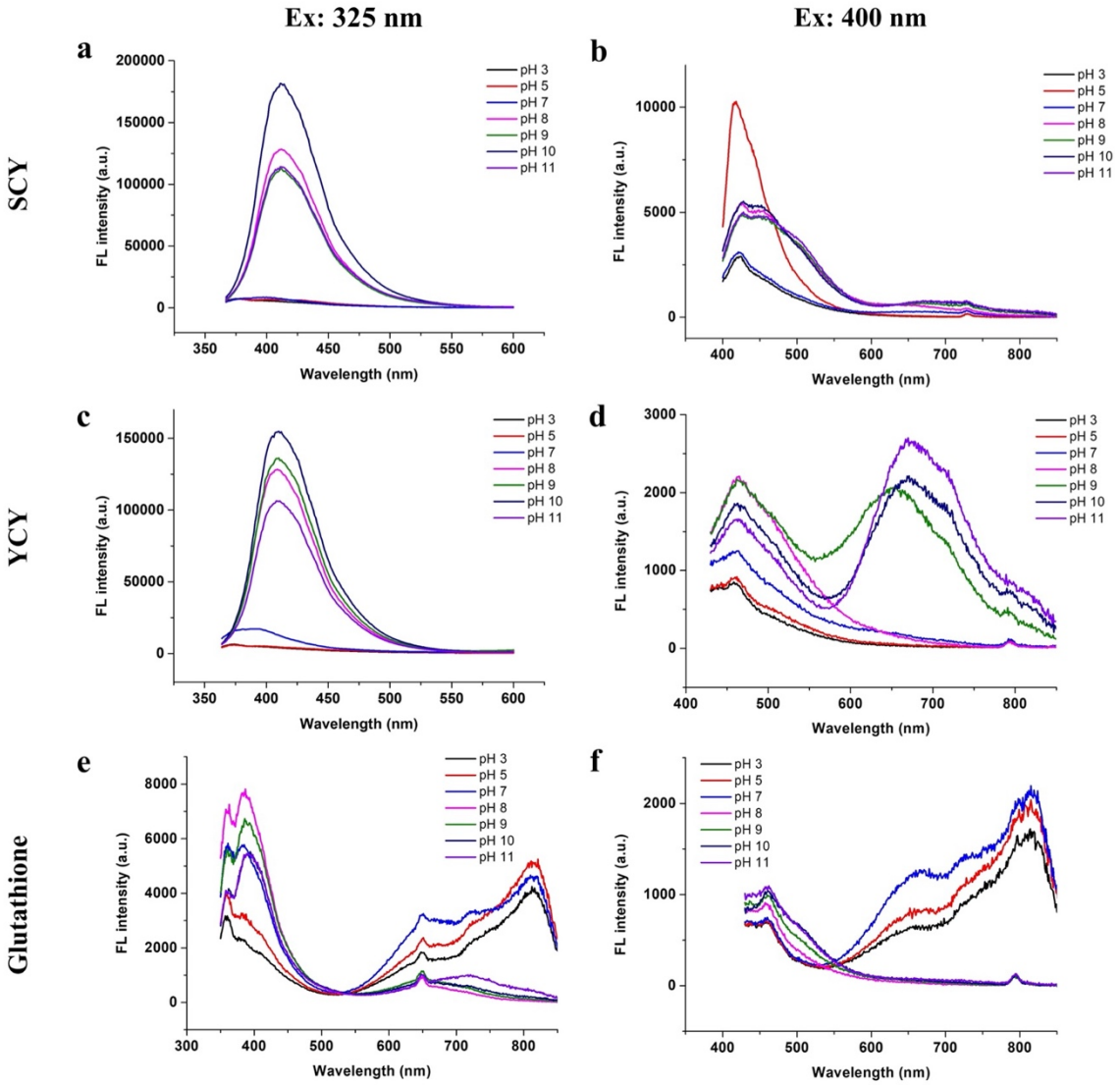

Figure 1. Fluorescent emission spectra of the crude AuNC solutions prepared by mixing with different peptides at the different pH conditions with 325 nm and 400 nm excitations. (a) and (b): SCY peptide. (c) and (d): YCY peptide. (e) and (f): glutathione.

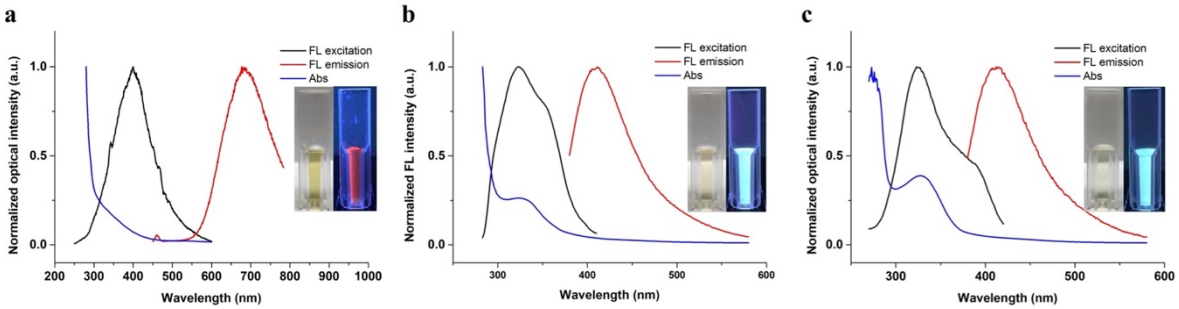

Figure 2. UV-Vis, fluorescent emission and excitation spectra of (a) Red-YCY-AuNC, (b) Blue-YCY-AuNC, and (c) Blue-SCY-AuNC [photographs: AuNC solutions under visible light (left) and 365 nm UV lamp (right)].

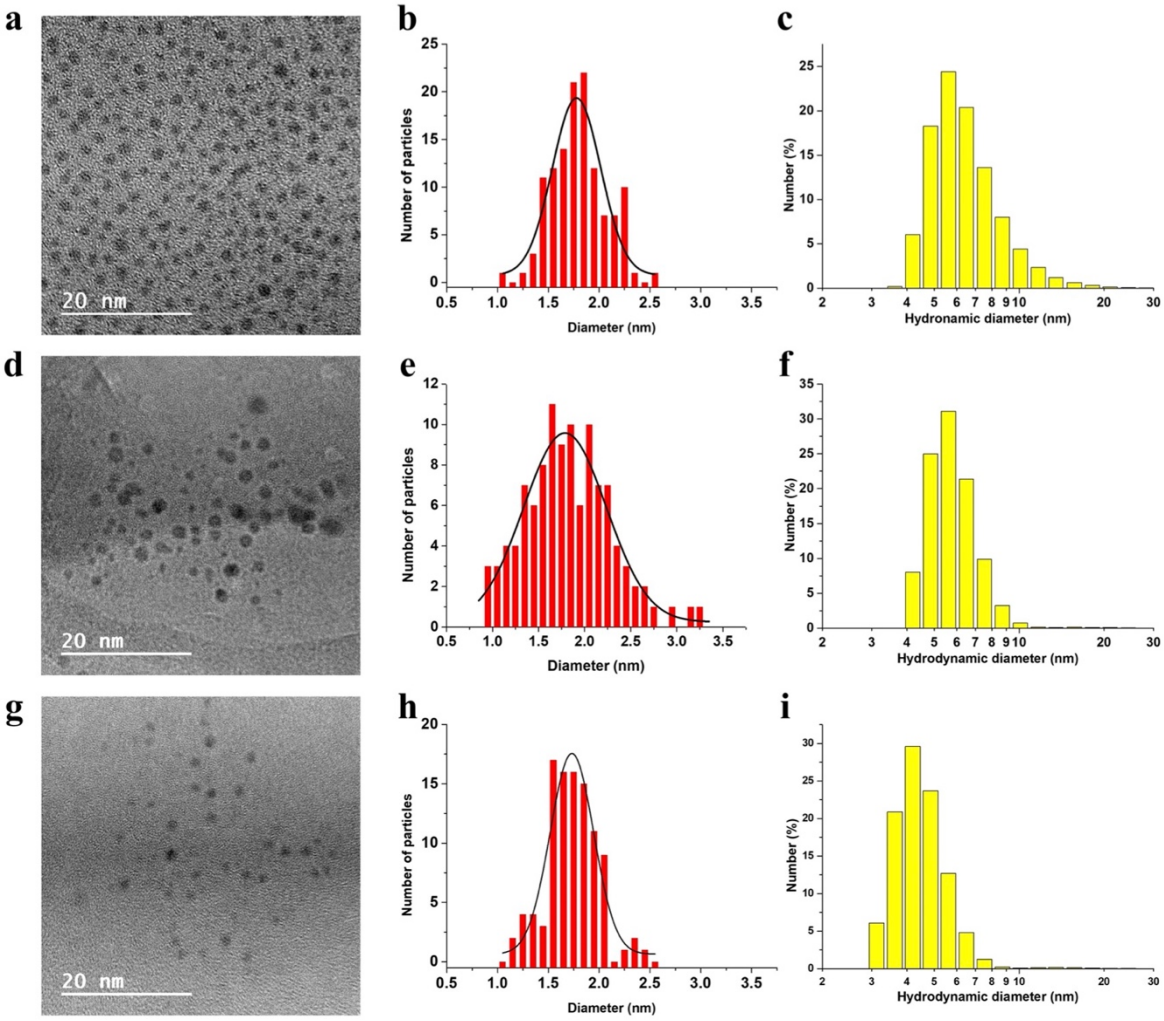

Figure 3. Red-YCY-AuNC: (a) TEM image, (b) size distribution histogram and (c) DLS histogram. Blue-YCY-AuNC: (d) TEM image, (e) size distribution histogram and (f) DLS histogram. Blue-SCY-AuNC: (g) TEM image, (h) size distribution histogram and (i) DLS histogram.

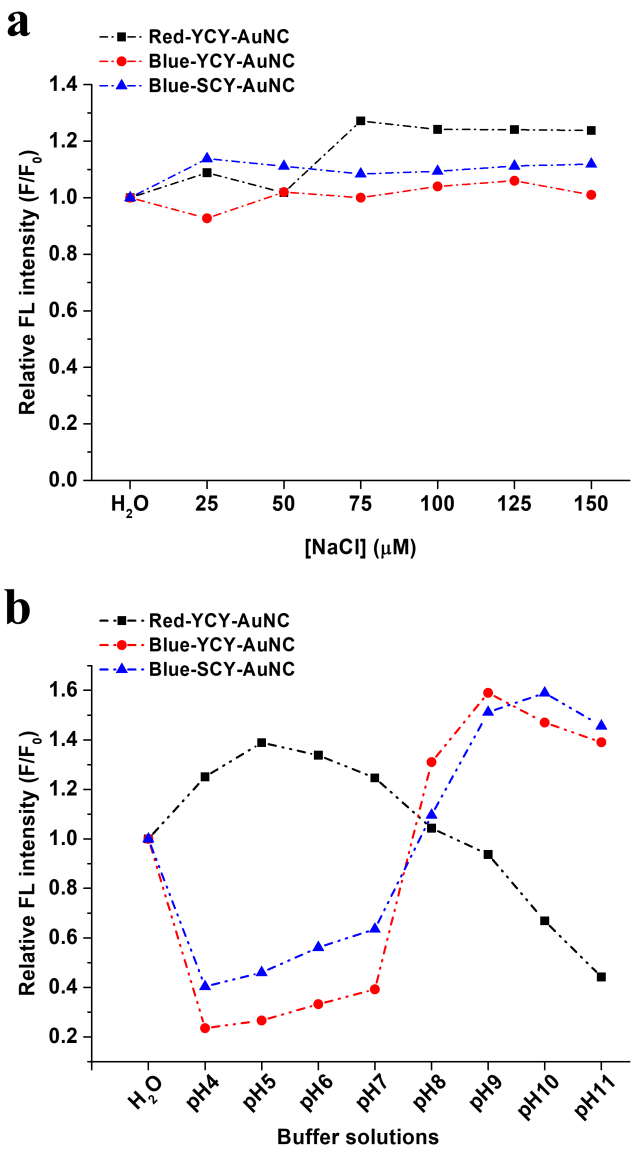

Figure 4. (a) Relative fluorescence intensity of Blue-YCY-AuNC, Blue-SCY-AuNC (λ_{ex}: 325 nm, λ_{em}: 415 nm) and Red-YCY-AuNC ((λ_{ex}: 400 nm, λ_{em}: 675 nm) after mixing with various concentration of NaCl (NaCl concentration shown on x-axis is after mixing). (b) Relative fluorescence intensity of Blue-YCY-AuNC, Blue-SCY-AuNC (λ_{ex}: 325 nm, λ_{em}: 415 nm) and Red-YCY-AuNC ((λ_{ex}: 400 nm, λ_{em}: 675 nm) at different pH.

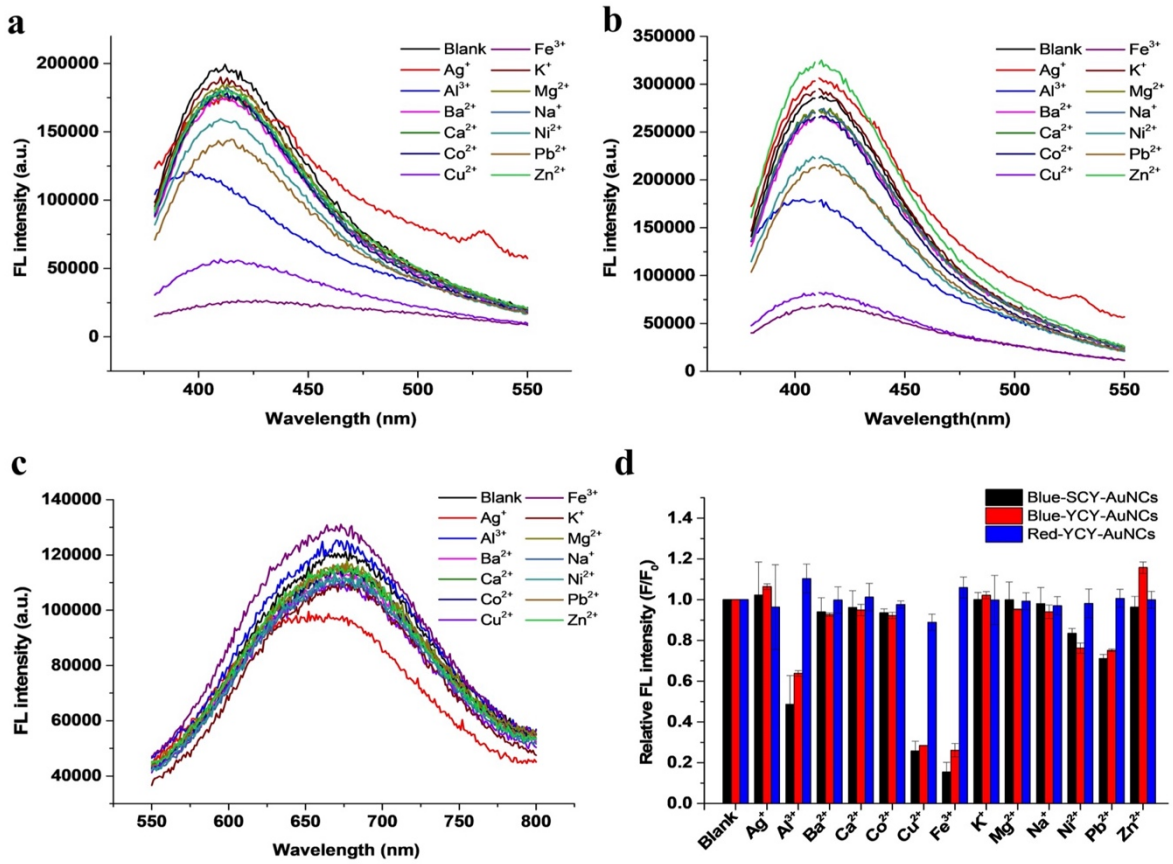

Figure 5. Fluorescence spectra of (a) Blue-YCY-AuNC, (b) Blue-SCY-AuNC, and (c) Red-YCY-AuNC after mixing with 13 different metal ions (50 μM, excitation at 325 nm and 400 nm for blue fluorescence-emitting AuNCs and red fluorescence-emitting AuNC respectively). Metal incubation time was 2 min. (d) Histogram plot of fluorescence quenching of each AuNC caused by 13 different meal ions. The error bars represent standard deviation from three independent measurements.

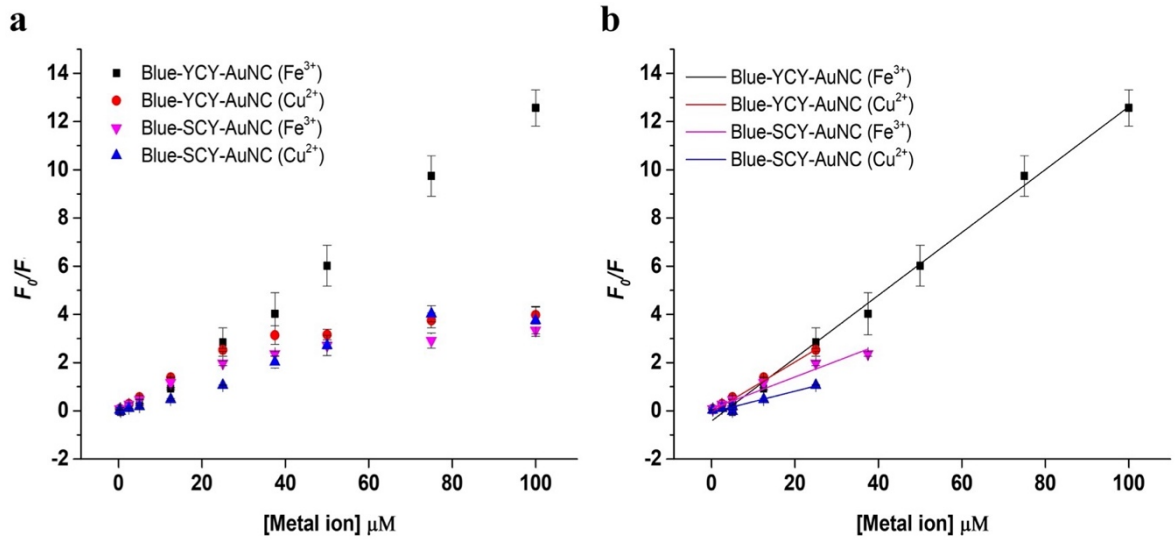

Figure 6. (a) Plot of F_0/F at 415 nm versus the concentration of Fe^{3+} and Cu^{2+}. (b) Stern-Volmer plot of Blue-YCY-AuNC and Blue-SCY-AuNC against Fe^{3+} (Blue-YCY-AuNC: 0.25 – 100 μM, Blue-SCY-AuNC: 0.25 – 37.5 μM) and Cu^{2+} (Blue-YCY-AuNC: 0.25 – 25 μM, Blue-SCY-AuNC: 0.25 – 25 μM). Excitation was at 325 nm. The error bars represent standard deviation from three independent measurements.

Sample	Detection metal ion	Slope & intercept	R^2	Linear detection range (μM)	Limit of Detection (μM)
Blue-YCY-AuNC	Fe^{3+}	$Y=0.128\boldsymbol{x} - 0.314$	0.995	0.25 - 100	3.2
	Cu^{2+}	$Y=0.101\boldsymbol{x} + 0.0533$	0.997	0.25 - 25	0.77
Blue-SCY-AuNC	Fe^{3+}	$Y=0.0646\boldsymbol{x} + 0.144$	0.965	0.25 - 37.5	4.1
	Cu^{2+}	$Y=0.0424\boldsymbol{x} - 0.0144$	0.993	0.25 -25	1.3

Table 1. Comparison of Blue-YCY-AuNC and Blue-SCY-AuNC for sensing Fe^{3+} and Cu^{2+}.

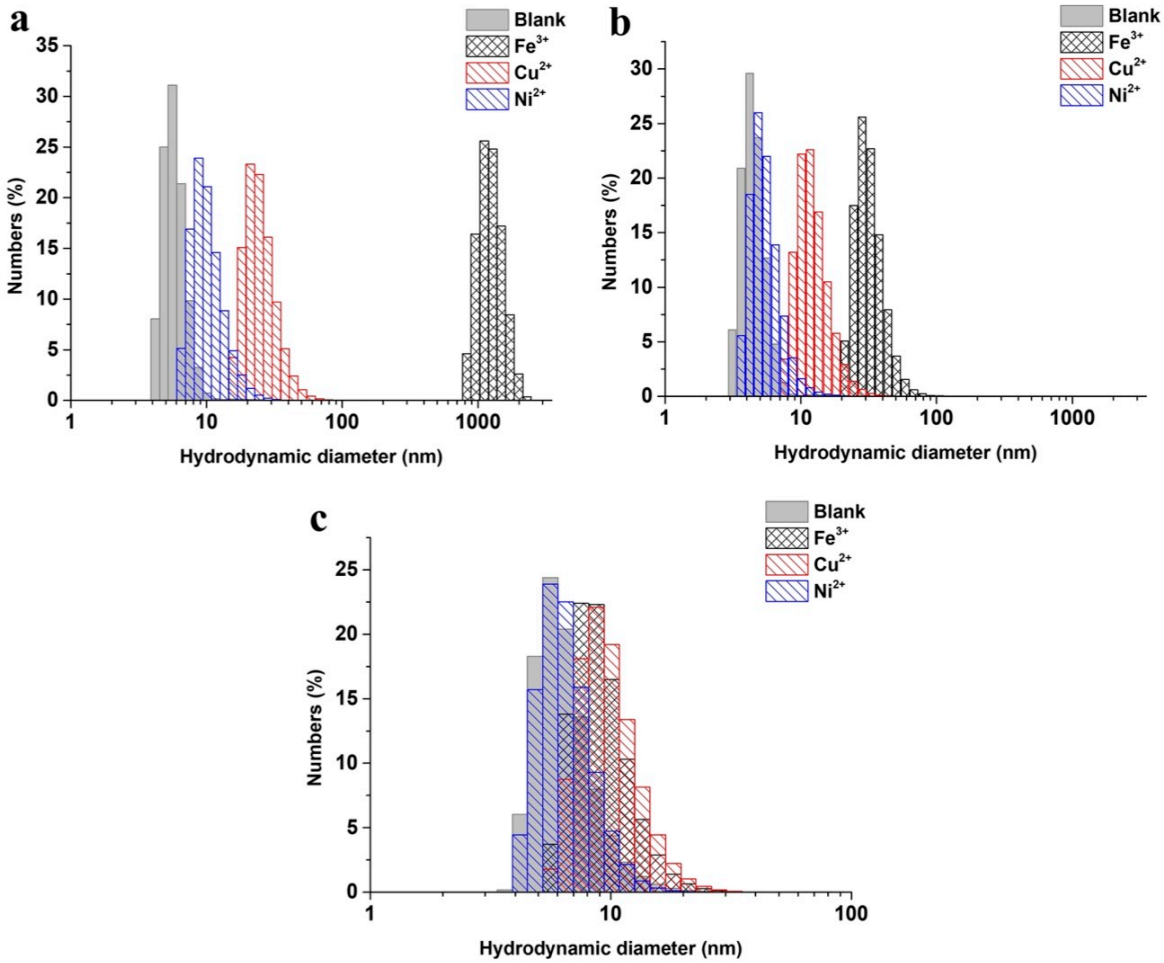

Figure 7. Analysis of hydrodynamic diameter of (a) Blue-YCY-AuNC, (b) Blue-SCY-AuNC, and (c) Red-YCY-AuNC before and after adding Ni^{2+}, Fe^{3+}, and Cu^{2+}.